We are IntechOpen, the world's leading publisher of Open Access books Built by scientists, for scientists

4,800
Open access books available

122,000
International authors and editors

135M
Downloads

Our authors are among the

154
Countries delivered to

TOP 1%
most cited scientists

12.2%
Contributors from top 500 universities

CLARIVATE ANALYTICS
BOOK CITATION INDEX
INDEXED

WEB OF SCIENCE™

Selection of our books indexed in the Book Citation Index
in Web of Science™ Core Collection (BKCI)

Interested in publishing with us?
Contact book.department@intechopen.com

Numbers displayed above are based on latest data collected.
For more information visit www.intechopen.com

Nanocomposite Films Deposition by means of Various Filtered Vacuum Arc Systems

Seunghun Lee[1], Do-Geun Kim[1], Igor Svadkovski[2] and Jong-Kuk Kim[1]
[1]Korea Institute of Materials Science,
[2]Belarussian State University of Informatics and Radioelectronics,
[1]Korea
[2]Belarus

1. Introduction

A hard coating is of considerable significance in industrial applications such as high speed cutting tools. The hard coating technologies have been investigated to improve a life time as well as performance of the tools. Up to now, TiN coatings were widely used. However, the substitution of TiN has been required because of its low oxidation temperature of 500 °C. From 1970s, it was revealed that nanocomposite films have their infinite probability enough to replace the previous materials such as TiN. Nanocomposite materials such as nanocrystalline TiN/Si_3N_4, $TiN/TiC/Si_3N_4$, and $TiN/AlN/Si_3N_4$ exhibited superior oxidation temperature (~1000 °C) as well as ultra hardness (45-55 GPa) [1-6].

Many deposition tools like a magnetron sputtering, plasma enhanced chemical vapor deposition (PECVD), arc ion plating (AIP), and filtered vacuum arc (FVA) were introduced for synthesizing nanocomposite films. Table 1 summarized previous works of nanocomposite coatings.

Nanocomposite films based on TiN were dominantly investigated with the incorporation of silicon or carbon. The incorporation methods such as an alloy arc cathode, addition of reactive gas, and additional magnetron sputtering were used to deposit ternary or quaternary composed nanocomposite films. The magnetron sputtering and PECVD have been firstly used to the growth of nanocomposite films due to the simplicity of controlling a composition ratio. Precise composition control of additional components is important. For example, Ti-Si-N nanocomposite films represent the maximum hardness at Si content of 9±1 at.%. After that, a vacuum arc discharge has been applied to the nanocomposite coatings because it can generate dense plasma with energetic ions near a cathode spot (<60 eV), which help a delicate crystallization and rapid growth. Nevertheless, the vacuum arc method cannot avoid the problem of macro particles emitted at an arc spot. The macro particles make some defects in the coatings and result in drastically decreasing corrosion resistance when the coatings are exposed in the corrosive environment. Therefore magnetic filters have been introduced to transport plasma except the macro particles. The filters only transport charged particles using electromagnetic fields and the neutral macro particles collide with a filter wall by an inertia drift. As a result, various FVA methods have been widely applied to the nanocomposite deposition.

Method	Material	Hardness	Ref.
Arc	Ti-Si-N	45 GPa	[7][9]
Arc	Ti-Al-N/Cr-N	37 GPa	[8]
Arc	Ti-Al-Si-N	34 GPa, 42.4 GPa	[10][11]
Arc	Ti-Al-N	35.5 GPa	[2]
Arc, magnetron sputter	TiN-Cu, CrN-Cu, MoN-Cu	27-42 GPa	[12]
Arc, magnetron sputter	Ti-Si-N	45-55 GPa	[13][15]
FVA, magnetron sputter	Ti-Si-N	45 GPa	[1]
FVA, magnetron sputter, E-beam evaporation	Ti-Cr-N,Ti-B-C	43.2 GPa	[14][17]
FVA	Ti-Si-N	40.1 GPa,	[16]
PECVD	Ti-Si-N	3500 HK(kg/mm^2), 40 GPa	[18][19]
PECVD	Ti-Si-C-N	48 GPa	[4]
PECVD	Ti-Si-C-N	52 GPa	[20]
Magnetron sputter	Ti-Si-N	38GPa, 45 GPa	[21][22]

*Arc=Cathodic arc evaporation, Arc ion plating
**FVA=Filtered vacuum arc

Table 1. Nanocomposite coatings by mean of various methods

2. Various FVA applications for nanocomposite coatings

2.1 Theory of FVA

Main issues of FVA are the efficient removal of the macro particles from plasma, and the minimum loss of ions through a filter wall. The effective approach to reduce the macro particles is based on the spatial separation of the trajectories of macro particles and ions [23]. If the magnetic field is curved such as the field inside a curved solenoid, electrons follow the curvature. Such electrons are said to be magnetized. In contrast, ions are usually not magnetized because the gyration radius of ion is much larger than that of electron and the characteristic radius of the filter. Nevertheless, ions are forced to follow the magnetic field lines due to the electric fields between electrons and ions. Therefore, plasma containing ions and electrons is transported along magnetic field lines [24].

It was shown that the plasma transport efficiency is limited by drifts caused by the centrifugal force and by the electric field in plasma [25]. Several studies have been conducted to determine the maximum efficiency and optimum condition for curved magnetic filters. An analysis of plasma motion along the toroidal magnetic field shows that plasma transported by the magnetic field in the plasma guiding duct should satisfy the following relation [26],

$$B > M_i V_o / Zea \qquad (1)$$

where M_i is the ion mass, V_o is the translational velocity, Z is the charge multiplicity of the ion, e is the electron charge, and a is the minor radius of the plasma guide. Transport of heavy metal ions having energy of even a few tens of electronvolts requires magnetic fields of above 1 Tesla to fulfill the inequality in Eq. (1). At these magnetic fields, however, it is

practically impossible to provide a stable burning of the direct current arc discharge. Besides the plasma injection into this field would also present certain difficulties. Therefore, it is reasonable to investigate heavy-element plasma flow transport in a curvilinear system with crossed electric and magnetic fields using the principles of plasma optics as a guide [27,28]. In this case, the required magnetic field is determined by the following condition, $\rho_e < a < \rho_i$, where ρ_e and ρ_i are the electron and ion Larmor radius, respectively. The required field is significantly lower than the fields defined by the expression in Eq. (1). Electron Larmor radius is

$$\rho_e = \left(m_e k T_e\right)^{1/2} / eB \tag{2}$$

where m_e is the electron mass, k is Boltzmann constant, and T_e is the electron temperature.

Note that electrons are only magnetized, while the ions are not. The electrons move along the magnetic field lines. In view of the high longitudinal conductivity of plasma, the magnetic field lines are equi-potentials. Considering a plasma diffusion in vacuum, electrons have higher mobility than ions due to their smaller mass except for a sheath boundary. However, electrons expand with the same velocity as ions because electrostatic forces keep the electrons and ions together. And a cross field diffusion is given by the Bohm formula, $D_B = kT_e/16B$, though the cross field diffusion coefficient, D, is proportional to B^{-2} in the classical theory [33]

Anders mentioned about the criterion of system efficient, K_s, which is generally considered as the ratio of the total ion flow at the exit of the system, I_i, to the arc discharge current, I_a, as follows,

$$K_s = I_i / I_a \ . \tag{3}$$

The system coefficient is typically 1% [24]. There is general agreement that the transport efficiency is maximized by focusing the plasma into the duct and biasing the duct to a potential of 20 V. Predictions of the available maximum transmission vary between 11 and 25% depending on the ion energy [29]. In practice, the transport of plasma produced by pulsed high current arcs (HCA) was showed that the system coefficient was 7% [24]. For linear FVA [30], the maximum value of the system efficiency reached 8% when arc current I_a was adjusted in the range of 100–110 A and the magnetic filter field was ~ 20 mT.

To supplement the accuracy of system coefficient, a particle system coefficient, K_p, is proposed to eliminate the influence of the various ion charge states by considering the mean ion charge state, Z_{av}, of the used metal.

$$K_p = I_i / Z_{av} I_a \tag{4}$$

Because the average ion charge state is taken into account, the particle system coefficient is more closely related to the deposition rate [31]. However this can be particularly insufficient for filter optimization when the system used a graphite cathode that generates solid rebounding macro particles.

The problem was solved by computing the particles trajectories using a two-dimensional approximation [32]. It was assumed that the macro particles were solid and spheres, the inner surfaces of the plasma guide and the intercepting fins were smooth, the repulsion of particles from the walls was partially elastic, the particles were emitted by the cathode spot with equiprobability in any direction, i.e. of angular macro particle flow density distribution

has the form $N(\alpha)=const$, where a is the angle between the normal to the cathode active surface and the direction of macro particle emission. The computation results make it possible to estimate the ratio of the exit macro particle flow N_{ex} to the flow N_{ent} generated by the cathode spot. The ratio N_{ex}/N_{ent} characterizes the likelihood of an macro particle passing through the system. The results of simulations indicate that the absence of a direct line-of-sight between the cathode and the substrate is not always sufficient to provide the required degree of macro particle removal from the plasma. The results of computations performed for various magnetic filters are presented in Table 2 [33].

Filter type	Knee (45°)	Torus (45°)	Rectang.	Dome	Torus (90°)	Retil.	Radial	Wide apert.
N_{ex}/N_{ent} [%] (predicted)	1.7	25.0	17.0	1.7	0	4.4	0	0
Transport [%] (measured)	3.0	2.5	2.5	2.5	1.5	1.8	8.4	~6.0

Table 2. Fitlering (N_{ex}/N_{ent}) and transporting properties of magnetic plasma filters [33]

2.2 Various types of FVA systems [34]

There are various types of filters as shown in Fig. 1. Most types are used magnetic fields to transport plasma without macro particles. Several types are only used the collisional reduction of macro particles. In most cases, the plasma is transported from the cathode to the substrate, and the droplets are eliminated by the plasma transportation wall. Many review papers of the filtered arc system and technology have been reported [35]–[42]. A typical filtered arc system with its different electromagnetic plasma transportation duct or droplet filter configurations is shown in Fig. 1(a)–(h). Electromagnetic coils transporting plasma in the out of line of sight direction can be positioned in the chamber, instead of placing them outside of the filter duct. The off-plane double bend filter [43], [44] is nicknamed FCVA and is now commercially available. Most FAD units have electromagnetic coils outside of the plasma duct and have baffles inside the duct wall. However, some types have freestanding coils inside the plasma duct or the chamber. Other interesting filters have been developed. Examples are shown in Fig. 1(i)–(l). In the Venetian-blind filter, the plasma passes between the vane lamellae, and the droplets are caught or reflected by the lamellae [45], [46]. A coaxial filter is operated with a large current pulse, and the plasma is driven by a self magnetic field [47]. An electrostatic filter can be used with a pulsed arc having a laser trigger [48]. However, recently only the laser triggered arc is used without the electrostatic filter. Mechanical filters can be used in a pulse arc [49], which may also be used in pulsed laser deposition [50].

2.3 FVA systems for nanocomposite films deposition

Various FVA methods were introduced to deposit ternary or quaternary composed nanocomposite films. A hybrid system consisting of FVA and magnetron sputter was widely used. In the hybrid system, FVA evaporates materials to be required a large amount such as Ti and the incorporated material like Si was used to the magnetron sputtering cathode. By controlling the power of magnetron sputter, the additional content of Si can be
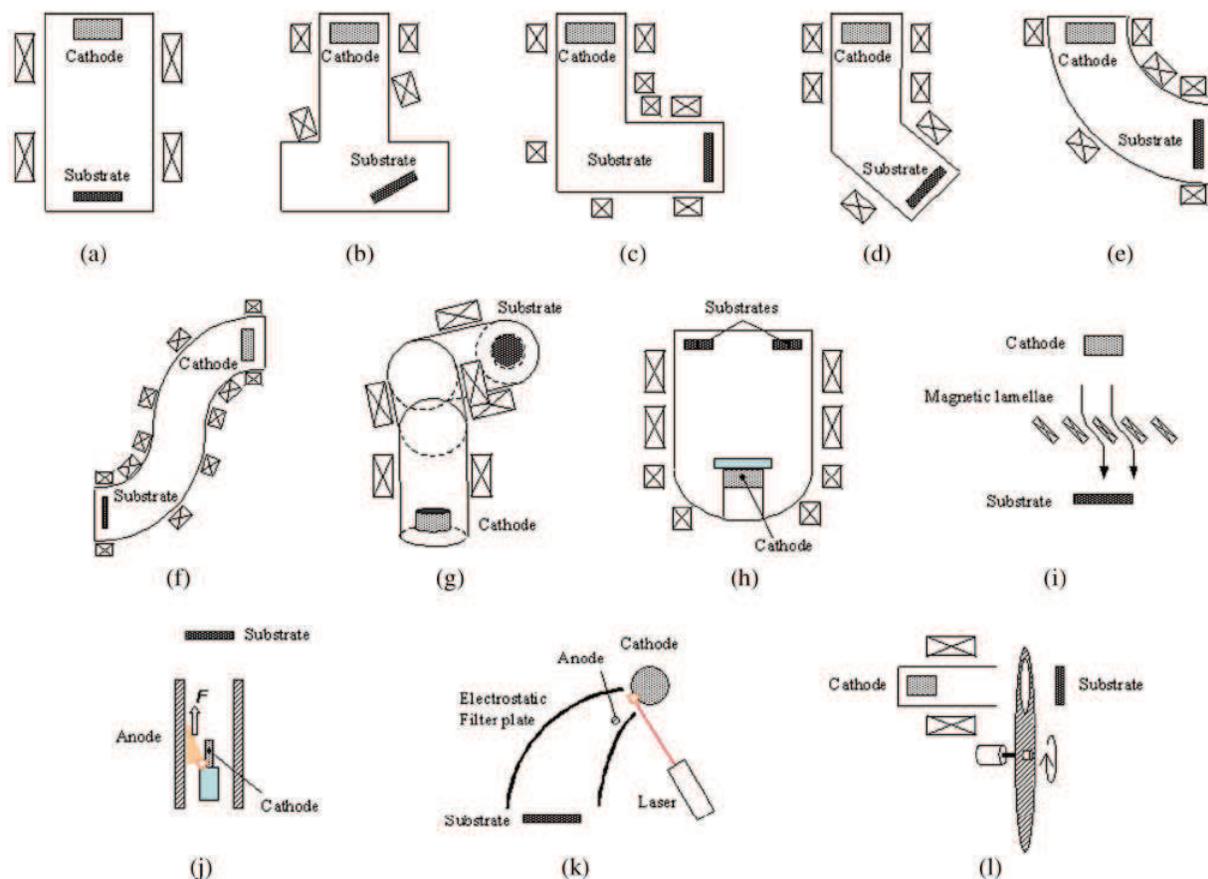
Fig. 1. Various types of filter systems [34]. (a) Rectilinear. (b) Bent. (c) Rectangular. (d) Knee. (e) Torus. (f) S-shape. (g) Off-plane double bend. (h) Dome. (i) Venetian blind. (j) Co-axial (pulse). (k) Electrostatic filter with laser trigger (pulse). (l) Mechanical pulse.

modulated. For example, Fig. 2 shows the schematic of hybrid system for nanocomposite coatings. The magnetron sputtering cathode is placed near the outlet of filter vacuum arc source. The use of two separated targets allowed an independent regulation and enabled the adjustment of Ti/Si ratio by varying the current of magnetron. However, the interference of magnetic field between FVA and magnetron sputter should be considered to obtain sufficient deposition rate. The closed geometry of magnetic field between the two sources will cause the loss of ions and the decrease on deposition rate.

Sintering or alloy arc cathode methods are useful way to deposit nanocomposite films if one knows the optimum composition of additional components and the optimized composition is in the available range for cathode sintering. For instance, Ti-Si sintering cathode can be used for nanocomposite $TiN/a\text{-}Si_3N_4$ coatings because the optimum content of Si for high hardness is in the possible range (~10%) for Ti-Si sintering. And Ti-Al (5:5) alloy cathode, which manufacturing is simple, can be used to nc-$TiN/AlN/a\text{-}Si_3N_4$ coatings since the composition of alloy target is good for realization of superior properties.

Additionally, the injection of additive gas is also another way to deposit nanocomposite films. Especially, metal-organic source such as hexamethyldisiloxane (HMDSO), hexamethyldisilazane (HMDS), and tetramethylsilane (TMS) could be used to Si source. The plasma density and ion energy are enough to dissociate metal-organic materials and continuously supply deposition precursors.
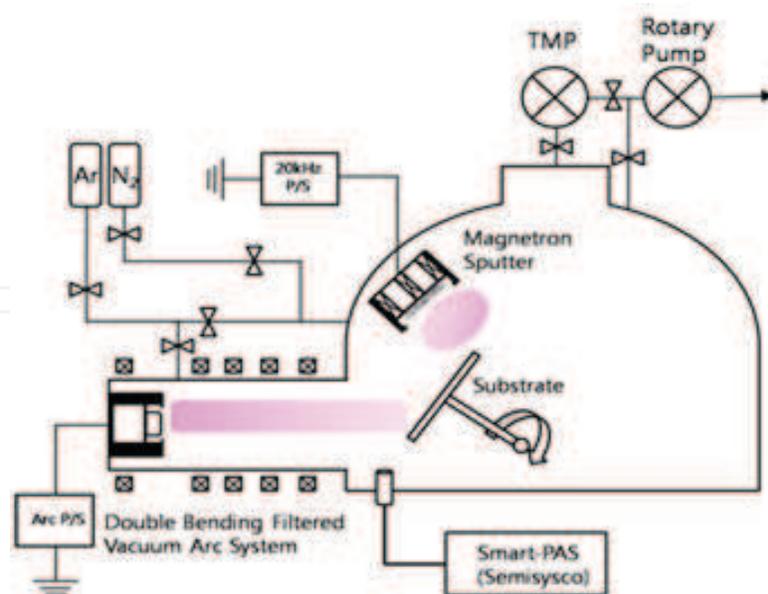
Fig. 2. A schematic of hybrid system.
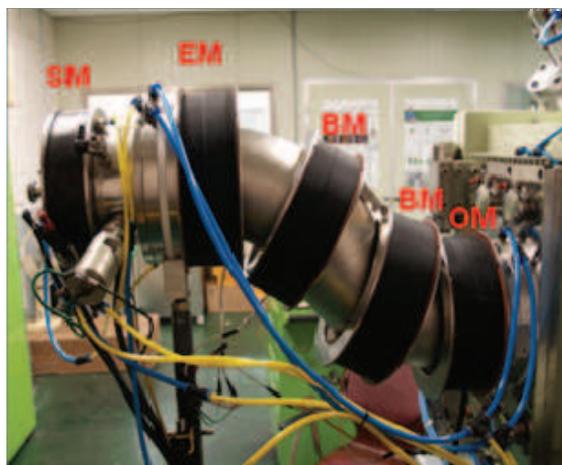
Fig. 3. S-shape filtered vacuum arc system.

3. Ti-Si-N/Ti-Al-Si-N nanocomposite film prepared by a FVA and unbalanced magnetron sputtering technique

3.1 Ti-Si-N/Ti-Si-Al-N nanocomposite films

Many investigations were carried out Ti–Si–N and Ti-Al-Si-N coatings due to its attractive physical and chemical properties, such as high hardness and good oxidation resistance. The coating layers with Si content of approximately 10 at.% shows very high hardness (more than 40 GPa) and those microstructures were characterized by nanocomposite consisting of nano-sized TiN or AlN crystallites embedded in amorphous silicon nitride matrix [15,51,52]. The nanocomposite coating layer also exhibited significantly improved oxidation resistance compared to that of TiN [53,54]. It was reported that the amorphous SiO_2 oxidized from Si_3N_4 played a major role as the oxidation barrier [55]. And the microstructure characterized by solid-solution of Al into TiN improved oxidation property [56,57]. With a decrease in grain size, the multiplication and mobility of the dislocations are hindered, and the hardness

of materials increases. Veprek [58] imbedded 4–11 nm TiN crystals in amorphous Si_3N_4 matrix and obtained a coating hardness of 50–70 GPa. Combination of two phases provides complex boundaries to accommodate coherent strain, which result in the increase of coating hardness [59].

3.2 System configuration for nanocomposite films deposition

Nanocomposite coatings were carried out by a filtered vacuum arc and an unbalanced magnetron (UBM) sputtering technique as shown in Fig.2. The filtered vacuum arc used the S-shape magnetic filter consisting of 5 magnetic coils to eliminate macro particles. The magnetic field inside the plasma duct was optimized using a numerical simulation to prevent the striking of the plasma stream onto the plasma duct. The average strength of the magnetic field was 15 mT and the diameter of the plasma duct was 15 cm. A Ti (99.8%) arc cathode (diameter: 8 cm) was used in Ti-Si-N coatings. A $Ti_{50}Al_{50}$ (99.8%) alloy cathode (diameter: 8 cm) was used in Ti-Al-Si-N coatings. The area of the Si UBM source was 400 cm^2 and placed next to the outlet of the plasma duct. The UBM power was released as a 20 kHz asymmetric pulse. The substrates were high speed steel. The substrate was heated by plasma and the substrate temperature was maintained ~ 200ºC for a deposition.

The coating process consisted of 3 steps, an ion bombardment cleaning, an interlayer deposition, and nanocomposite coating. In the ion bombardment cleaning, Ar ions were impinging into the substrate with the substrate bias of -600 V. Ar gas was introduced into the arc cathode while maintaining a pressure of 1 mTorr. In the interlayer deposition, the pressure decreases to 0.3 mTorr to enhance the ion transport into the substrate. After that, multi-components nanocomposite films were coated using a gas mixture of Ar (5 sccm) and N_2 (15 sccm). The dissipated powers of arc and magnetron sputter were 1.8 kW and 0–0.5 kW, respectively. Typical deposition conditions are shown in Table 3.

Base pressure	1.0×10^{-5} Torr	Arc current	60 A
Working pressure	6.0×10^{-4} Torr	Sputter current	0-1.5 A
Gas ratio	N_2:Ar=3:1	Substrate voltage	-20 V
Arc target	Ti or$Ti_{50}Al_{50}$	Rotational speed	25 RPM
Sputter target	Si (99.99%)	Working temperature	< 200 ºC

Table 3. Typical deposition conditions for Ti-Si-N nanocomposite coatings

3.3 Characteristics of Ti-Si-N nanocomposite films
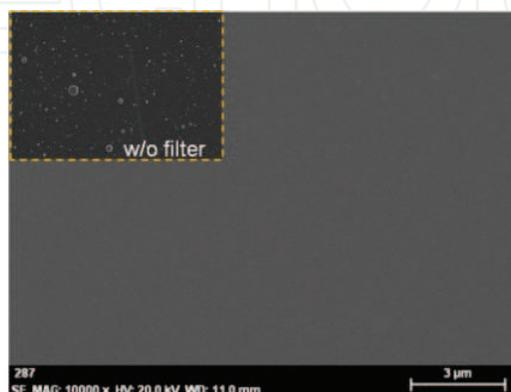
Fig. 4. Image of coated sample by scanning electron microscope without macro particles

Figure 4 shows the surface morphology of the sample prepared using the S-shape magnetic filter which removes macro particles during the deposition and the insert image indicates the surface morphology of the sample deposited by arc ion plating without the magnetic filter.
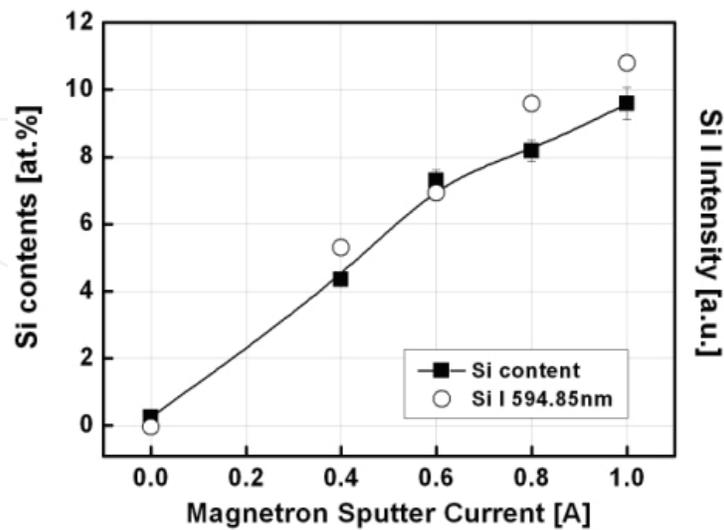
Fig. 5. Si contents as a variation of Si sputtering current and emission intensity of Si neutral (594.85 nm)

Figure 5 represents that Si content of the Ti–Si–N films as a function of magnetron sputtering system current. The composition data have been obtained by electron probe microanalysis. As magnetron sputter current increases from 0 to 1 A, Si contents increase up to level of 9.5%. This represents that Si contents can be easily controlled by the UBM power. Optical emission spectra of the Si neutrals (wavelength: 594.85 nm, energy: 7.17 eV→5.08 eV) from discharge also are proportional to the sputter current.
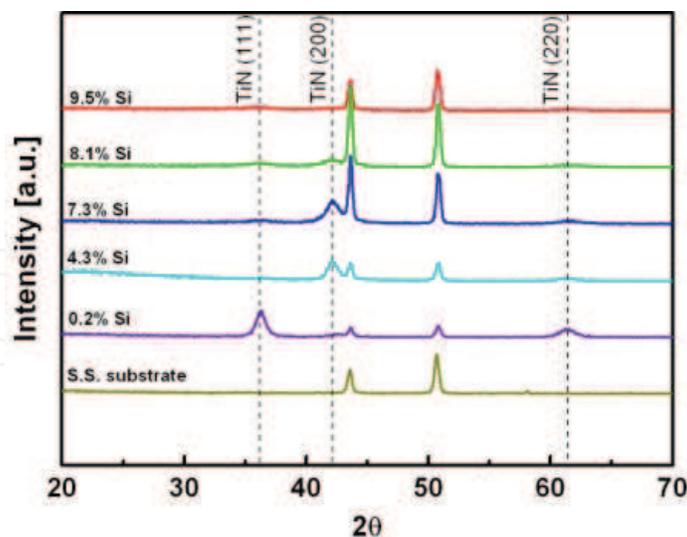
Fig. 6. X-ray diffraction patterns as a function of Si contents

Figure 6 shows the XRD patterns of Ti–Si–N coatings with different Si contents. The XRD patterns of Ti–Si–N coatings showed orientations of (111), (200), and (220) of TiN. These multiple orientations were in agreement with other Ti–Si–N coating layers [13,14]. However, any peaks corresponded to crystalline Si_3N_4 or titanium silicide phase were not observed. It

was estimated that Si was present in an amorphous phase of silicon or silicon nitride. The TiN peak intensity gradually reduced and a broadening phenomenon of peaks was observed with increasing Si content in Ti–Si–N films. XRD analysis represents that crystalline TiN (111), (220) is changed to crystalline (200) as Si content increases. Such XRD peaks behavior was believed due to generally decreasing of TiN grain size with increase of Si content. The result indicates that Ti–Si–N coatings have been characterized as nanocomposites, consists of TiN crystallites and amorphous Si_3N_4. If Si contents increases further, crystalline TiN becomes weaker and Si rich amorphous structure becomes dominant structure.
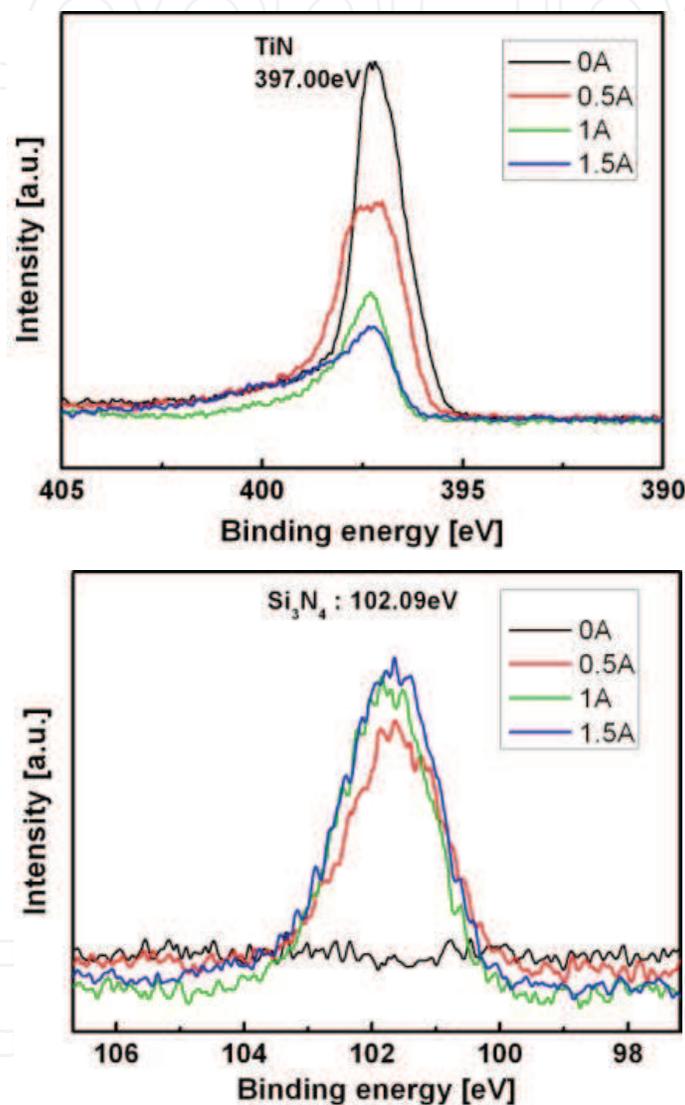
Fig. 7. X-ray photoelectron spectroscopy of Ti-Si-N coatings (1) Si 2p (2) N 1s

Figure 7 shows high-resolution XPS spectra of Si 2p (a) and N 1s (b) for Ti–Si–N coatings with different sputter currents. The binding energy of Si 2p at 101.8 eV corresponded of the data for stoichiometric Si_3N_4 [60, 61]. It should be note that, in spite of peak of 101.8 eV increased with increasing Si content in Ti–Si–N coating, there is not another peak corresponding to free Si at the binding energy of 99.3 eV. XPS analysis also shows that increase of Si content causes the weaker crystalline TiN bond status. This result is similar to XRD peak variation due to Si content variation. Precision control and determination of grain size is very important for nanocomposite coating.
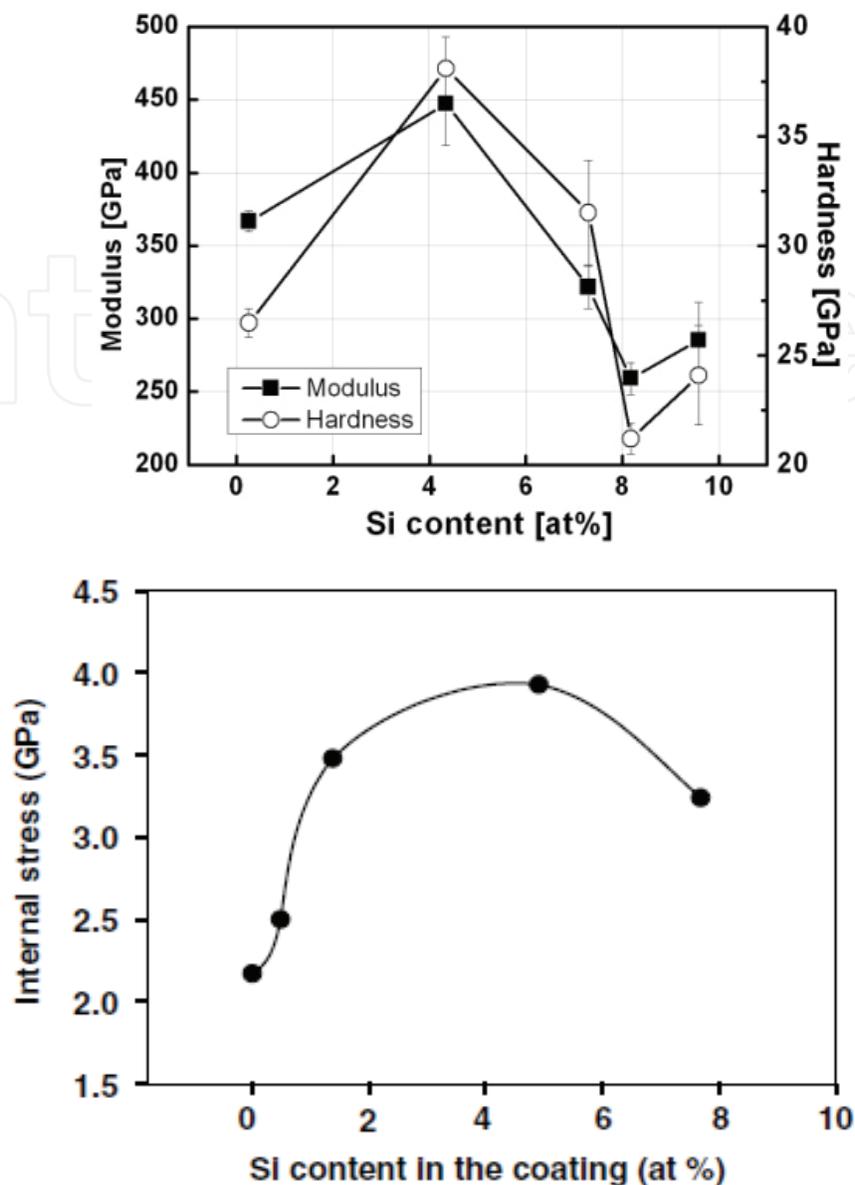
Fig. 8. (a) Micro hardness and modulus (substrate temperature: 200 ºC, bias voltage: -75 V) [1] (b) internal stress (substrate temperature: 350 ºC, bias voltage: -40 V) [62] as a function of the Si content in the coatings

Figure 8 shows micro hardness and modulus of Ti-Si-N coatings from Ref. [1] and internal stress from Ref [62] as a function of the Si contents. The increase in the Si content in the Ti-Si-N coatings from 0 at% to 4.3 at% results in a drastic increase in the micro hardness from 25 to 38 GPa. Then the micro hardness decreases to 23 GPa with a further increase in the Si content to 9.3 at%. The internal stress also has the maximum value of 4 GPa at Si content of ~ 5 at%. The Si incorporation causes the embedded amorphous Si_3N_4 phase surrounding nano-crystalline TiN phase. This induces the increase in micro hardness as well as the internal stress by the nanocomposite structure. Further Si addition, however, causes the decreases in the hardness. It has been proposed that the internal stress in the coating is strongly correlated with the defects, which cause the deformation and distortion of the lattice [63]
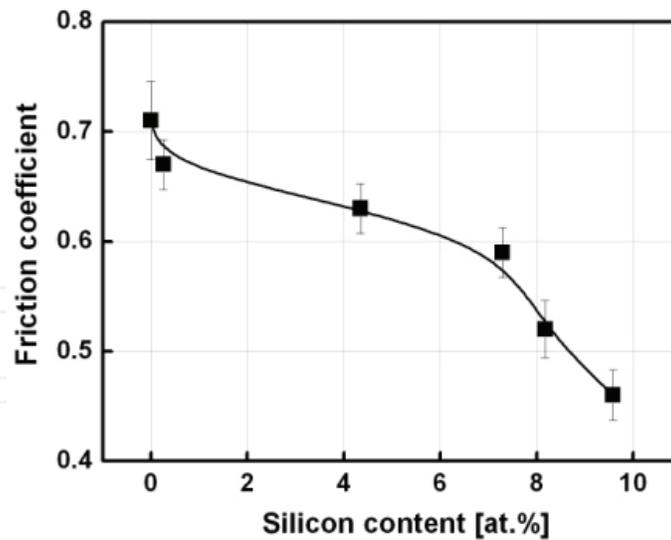
Fig. 9. Friction coefficient of Ti-Si-N films with various Si contents

In Fig. 9, the friction coefficient of Ti-Si-N films has lower value when Si incorporation is increased. The friction coefficient was decreased by the self-lubricating layer effect induced by SiO_2 or $Si(OH)_2$. Note that the self-lubricating effect is dominantly affected by ambient humidity the addition of Si into the coatings led to a continuous decrease in the grain size, which increased the defect density in the coatings.
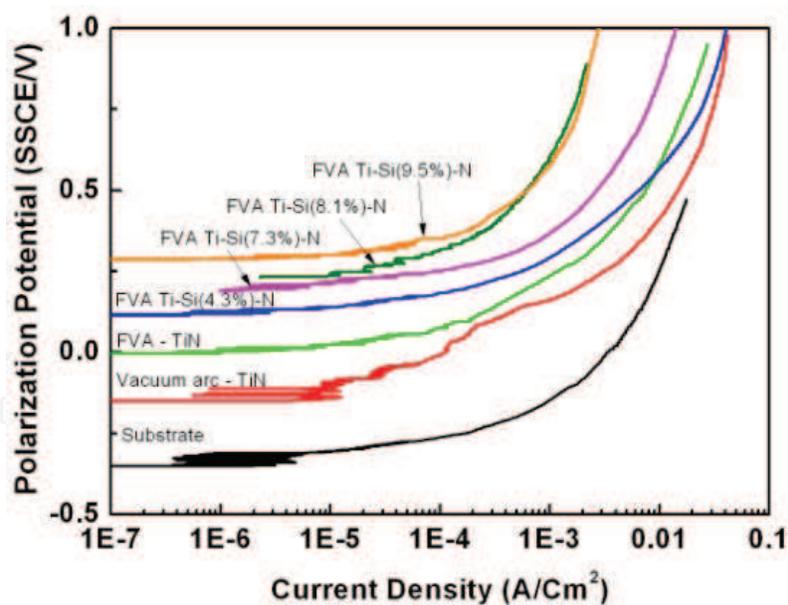
Fig. 10. Polarization voltage (Corrosion resistance) of Ti-Si-N films with various Si contens

Figure 10 shows the corrosion behavior of Ti-Si-N nanocomposite films. The coating samples of vacuum arc shows the worst polarization voltage because macro particles exist on the surface. The crack between the particle and the coating induces worse corrosion resistance. In case of FVA, the polarization voltage is increased due to the lack of macro particles. As Si incorporation was increased, the decreased grain size hinders the corrosion progress and the polarization voltage was increased.

3.4 Characteristics of Ti-Al-Si-N nanocomposite films
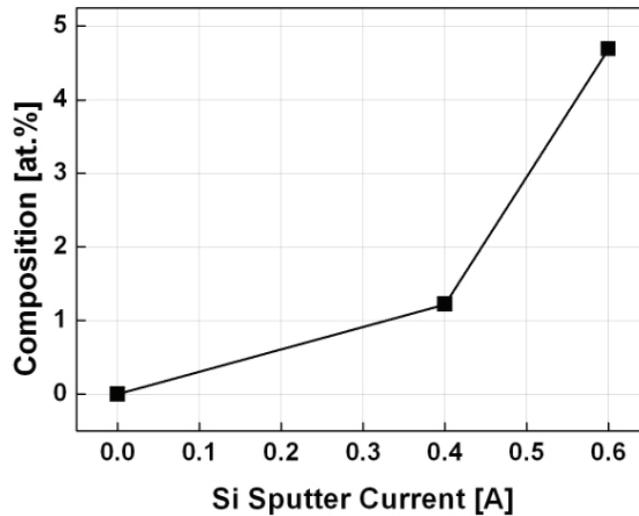
Fig. 11. Si contents as a function of Si UBM current.

Figure 11 shows the EPMA results when the Si contents were 0.04 at%, 1.22 at%, and 4.69 at% as the Si sputtering currents were 0 A, 0.4 A, and 0.6 A, respectively. The compositional analysis of the coating is carried out from electron probe microanalysis (EPMA, EPMA1600, Shimadzu). This means that the controlling of the Si content is available by the modulation of the Si sputter current. In the hybrid coating system consisting of the vacuum arc and the magnetron sputter, the ease of controlling the Si content in the multi components coating has been previously reported in other papers [1,64]. The non-linear increase on the Si contents could be induced by the discharge enhancement near the substrate due to the UBM discharge.
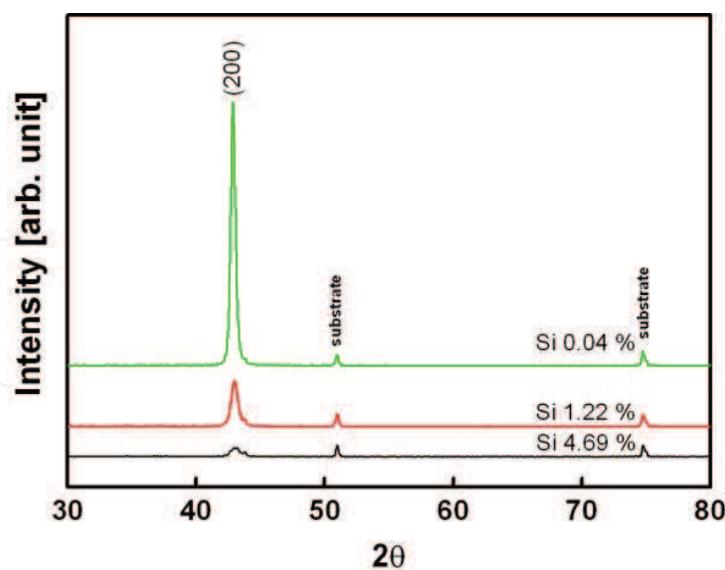
Fig. 12. X-ray diffraction patterns of Ti-Al-Si-N films

Figure 12 represents XRD patterns with various atomic percentages of Si. X-ray diffraction (XRD) with CuK$_\alpha$ radiation (X'Pert PRO macro particleD, Philips) was used to confirm the crystal phase. A crystal phase corresponding to a cubic TiN with a NaCl-type B1 structure was observed. There were no signals from silicon nitride or titanium silicide. The crystal plane of

(200) was observed continuously and the peak of the (200) plane becomes broader and smaller as the Si contents were increased from 0.04 to 4.69 at %. The broadening of the diffraction patterns implies the decrease of the grain size. The grain size evaluated by Scherrer's equation decreased from 9 nm to 7.5 nm as the Si content increased. The reduced grain size means the formation of amorphous Si_3N_4 between the crystalline TiAlN structures and this phenomenon is similar to the effect of the Si incorporation on the Ti-Si-N film [1]. In comparison with the Ti-Al-Si-N films prepared by a normal vacuum arc system with a heated substrate, there are no diffraction patterns of (111), (220), (311) and (222) planes in our results [65]. The low energy of incident ions and radicals by the self-bias and non-heated substrate induced the low mobility of the precursors and prevented the crystallization of TiN.
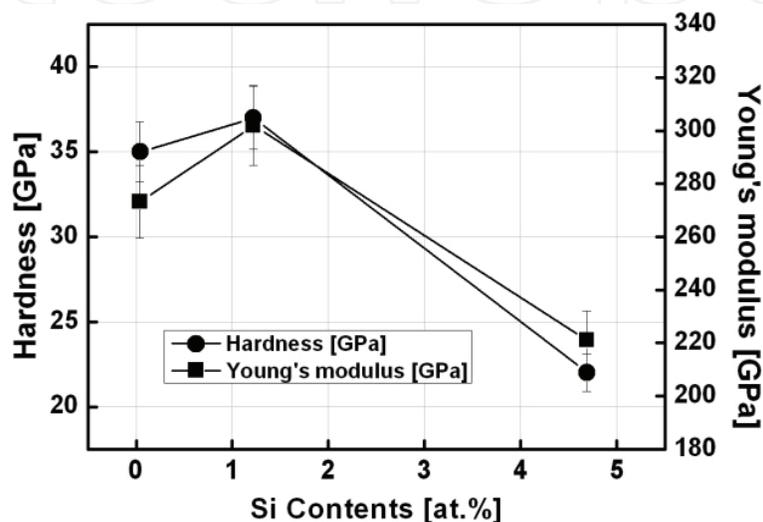
Fig. 13. Hardness and Young's modulus of Ti-Al-Si-N films

The micro hardness and Young's modulus of Ti-Al-Si-N coatings are shown in Fig. 13. A nanoindentation tester (MTS, Nanoindentation XP) equipped with a Berkovich diamond indentor was used to measure the micro hardness, averaged from 25 points. The displacement rate of the indentor was 0.2 nm/s until a depth of 100 nm was reached. As the Si contents increased until 4.69 at.%, the micro hardness and Young's modulus increased from 35 GPa and 270 GPa to 37 GPa and 300 GPa, respectively. However they became lowered to 22 GPa and 220 GPa, respectively, when the Si contents increased to 4.69 at.%. In comparison with the micro hardness of Ti-Al-N films, at ~30 GPa, the hardness of the films enhanced slightly with the incorporation of Si [66]. The nanocomposite structure consisting of the inter phase boundary between the crystalline Ti-Al-N and the amorphous Si_3N_4 phases should help account for the enhancement of hardness. The micro hardness of Ti-Al-Si-N [65] deposited by the normal vacuum arc system is higher than that of Ti-Al-Si-N prepared by our system. As mentioned previously when discussing the XRD patterns, the low mobility at the surface due to the low temperature of the substrate could not be effective to synthesize the crystallized nc-TiAlN.

Figure14 shows the H^3/E^{*2} values of Ti-Al-Si-N films as a function of the Si contents. The effective Young's modulus, $E^*=E/(1-v^2)$, and H^3/E^{*2} value were calculated from the results of Fig.13 with the assumption of Poisson ratio, v=0.25. The H^3/E^{*2} value is known to be proportional to the resistance to plastic deformation of hard materials [67]. The highest H^3/E^{*2} value was obtained at the Si content of 4 at.%. The highest resistance to plastic deformation of that film could be related to preventing dislocation formation or movement
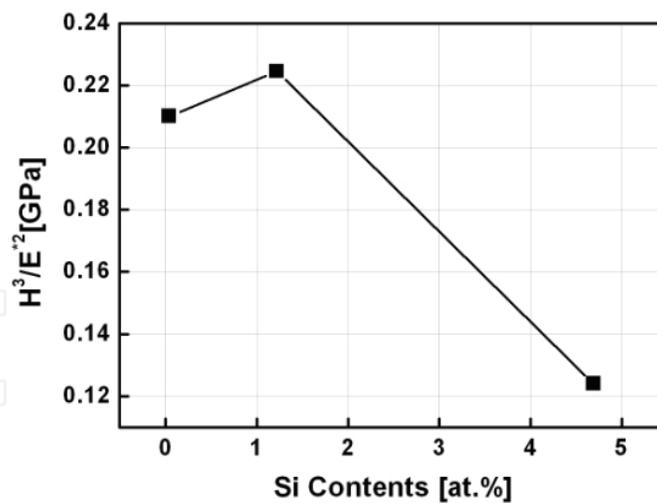
Fig. 14. H^3/E^{*2} ratios of Ti-Al-Si-N films

due to the nano-sized (Ti,Al,Si)N crystallites and the strong inhibition of crack propagation in amorphous Si_3N_4 under a high applied load [65,68].

4. Concluding remark

Nanocomposite materials could be synthesized using filtered vacuum arc applications. TiN based nanocomposite films were actively investigated until now and will be studied further. Another MeN/metal nanocomposite films such as ZrN-Cu were also reported that it has superior hardness and thermal stability [69]. FVA can be used to the other nanocomposite films and has promising probability as a deposition tool.

To use the FVA for industrial applications, a uniform coating technology is required to fulfill the standard of productivity. Methods of sweeping magnetic field and multi FVA systems have been investigated for uniform coatings in large area and more investigations are required continuously.

5. Reference

[1] Do-Geun Kim, Igor Svadkovski, Seunghun Lee, Jong-Won Choi and Jong-Kuk Kim, Current Applied Physics 9 (2009) S179–S181
[2] J. Bujak, J. Walkowicz and J. Kusinski, Surf. Coat. Technol.180 –181 (2004) 150–157
[3] P.J. Martina, A. Bendavida, J.M. Cairneyb and M. Hoffmanb, Surf. Coat. Technol. 200 (2005) 2228– 2235
[4] S.L. Ma, D.Y. Ma, Y. Guo, B. Xu, G.Z. Wu, K.W. Xu and Paul K. Chu, Acta Materialia 55 (2007) 6350–6355
[5] PalDey S, Deevi SC., Mater. Sci. Eng. A 342 (2003) 58–79.
[6] L. Chen, Yong Du, Ai J.Wang, She Q. Wang and Shu Z. Zhou, Int. Journal of Refractory Metals & Hard Materials 27 (2009) 718–721
[7] Sheng-Min Yang, Yin-Yu Chang, Da-Yung Wang, Dong-Yih Lin, WeiTe Wu, Journal of Alloys and Compounds 440 (2007) 375–379
[8] Yin-Yu Chang, Da-Yung Wang, Chi-Yung Hung, Surf. Coat. Technol. 200 (2005) 1702 – 1708

[9] A. Flink, T. Larsson, J. Sjolen, L. Karlsson, L. Hultman, Surf. Coat. Technol. 200 (2005) 1535 – 1542

[10] Y. Tanaka, N. Ichimiya, Y. Onishi, Y. Yamada, Surf. Coat. Technol. 146 –147 (2001) 215–221

[11] Li Chen, Yong Du, Ai J. Wang, She Q. Wang, Shu Z. Zhou, Int. Journal of Refractory Metals & Hard Materials 27 (2009) 718–721

[12] A. Ozturk, K.V. Ezirmik, K. Kazmanl, M. Urgen, O.L. Eryılmaz, A. Erdemir, Tribology International 41 (2008) 49–59

[13] Sung Ryong Choi, In-Wook Park, Sang Ho Kim, Kwang Ho Kim, Thin Solid Films 447 –448 (2004) 371–376

[14] V.I. Gorokovsky, C. Bowman, P.E. Gannon, D. Van Vorous, A.A. Voevodin, C. Muratore, Y.S. Kang, J.J. Hu, Wear 265 (2008) 741–755

[15] Kwang Ho Kim, Sung-ryong Choi, Soon-young Yoon, Surf. Coat. Technol. 298 (2002) 243–248

[16] Chi-Lung Chang, Jun-Han Chen, Pi-Chuen Tsai, Wei-Yu Ho, Da-Yung Wang, Surf. Coat. Technol. 203 (2008) 619-623

[17] V. Gorokhovsky, C. Bowman, P. Gannon, D. VanVorous, A.A. Voevodin, A. Rutkowski, C. Muratore, R.J. Smith, A. Kayani, D. Gelles, V. Shutthanandan, B.G. Trusov, Surf. Coat. Technol. 201 (2006) 3732–3747

[18] In-Wook Park, Kwang Ho Kim, Journal of Materials Processing Technology 130–131 (2002) 254–259

[19] Eung-Ahn Lee, Kwang Ho Kim, Thin Solid Films 420 –421 (2002) 371–376

[20] Yan Guo, Shengli Ma, Kewei Xu and Tom Bell, Nanotechnology 19 (2008) 215603

[21] Soo Hyun Kim, Jong Kuk Kim, Kwang Ho Kim, Thin Solid Films 420 –421 (2002) 360–365

[22] L. Rebouta, C.J. Tavares, R. Aimo, Z. Wang, K. Pischow, E. Alves, T.C. Rojas, J.A. Odriozola, Surf. Coat. Technol. 133-134 (2000) 234-239

[23] I.I. Aksenov, V.E. Strel'nitskij, V.V. Vasilyev, D.Yu. Zaleskij. Surf. and Coat. Technol. 163 –164 (2003) 118–127

[24] D.M. Sanders, A. Anders. Surf. Coat. Technol.133-134 (2000) 78-90.

[25] R.L. Boxman, V. Zhitomirsky, B. Alterkop, E. Gidalevich, I. Beilis, M. Keidar, S. Goldsmith.. Surf. Coat. Technol. 86-87 (1996) 243-253.

[26] N.A. Khizhnyak, Sov. Phys. Technol. Phys. 35 (1965) 847.

[27] I.I. Aksenov, V.A. Belous, V.G. Padalka, USSR Authors Certificate No. 605425, 1978, (Rus.).

[28] I.I. Aksenov, et al., Prib. Tekhn. Ehksp. 5 (1978) 236 (Rus.).

[29] P.J. Martin, A. Bendavid. Thin Solid Films 394 (2001) 1-15.

[30] I.I. Aksenov, V.V. Vasilyev, B. Druz, A.A. Luchaninov, A.O. Omarov, V.E. Strel'nitskij. Surf. Coat. Technol. 201 (2007) 6084–6089.

[31] E. Byon, J.-K. Kim, S.-C. Kwon, A. Anders. IEEE Trans. Plasma Sci., 23 (2004) 433-439.

[32] I.I. Aksenov, D.Yu. Zaleskij, V.E. Strel'nitskij, 1st International Congress on Radiation Physics, High Current Electronics and Modification of Materials, September, Tomsk, Russia. Proceedings3, 2000, p.130.

[33] A. Anders, S. Anders and I.G. Brown. Plasma Sources Sci. Technol. 4 (1995) 1-12.

[34] Hirofumi Takikawa, and Hideto Tanoue, *IEEE Trans. Plasma Sci.*, vol. 35, no. 4, pp. 992-999, Aug. 2007.

[35] D. A. Karpov, *Surf.Coat. Technol.*, vol. 96, no. 1, pp. 22–33, Nov. 1997.

[36] P. J. Martin, A. Bendavid, and H. Takikawa, *J. Vac. Sci. Technol. A, Vac. Surf. Films*, vol. 17, no. 4, pp. 2351–2359,Jul. 1999.

[37] A. Anders, *Surf. Coat. Technol.*, vol. 120/121, pp. 319–330, 1999.

[38] D. M. Sanders and A. Anders, *Surf. Coat. Technol.*, vol. 133/134, pp. 78–90, 2000.

[39] P. J. Martin and A. Bendavid, *Surf. Coat. Technol.*, vol. 142–144, pp. 7–10, 2001.

[40] A. Anders, *Vacuum*, vol. 67, no. 3/4, pp. 673–686, Sep. 2002.

[41] I. I. Aksenov, V. E. Strel'nitskij, V. V. Vasilyev, and D. Y. Zaleslij, *Surf. Coat. Technol.*, vol. 163/164, pp. 118–127, 2003.

[42] P. J. Martin and A. Bendavid, *Thin Solid Films*, vol. 394, no. 1/2, pp. 1–5, Aug. 2001.

[43] X. Shi, B. K. Tay, H. S. Tan, E. Liu, J. Shi, L. K. Cheah, and X. Jin, *Thin Solid Films*, vol. 345, no. 1, pp. 1–6, May 1999.

[44] B. K. Tay, Z. W. Zhao, and D. H. C. Chua, *Mater. Sci. Eng. R*, vol. 52, no. 1–3, pp. 1–48, May 2006.

[45] A. I. Ryabchikov and I. B. Stepanov, *Rev. Sci. Instrum.*, vol. 69, no. 2, pp. 810–812, Feb. 1998.

[46] O. Zimmer, *Surf. Coat. Technol.*, vol. 200, no. 1–4, pp. 440–443, Oct. 2005.

[47] S. Y. Chun, A. Chayaraha, A. Kinomura, N. Tsubouchi, C. Heck, Y. Horino, and H. Fukui, *Jpn. J. Appl. Phys.*, vol. 38, no. 4B,pp. L467–L469, Apr. 1999.

[48] C. F. Meyer and H.-J. Scheibe, presented at the Int. Conf. Metallurgical Coatings Thin Films (ICMCTF), San Diego, CA, 1999, Paper B4-9.

[49] Y. Taki, T. Kitagawa, and O. Takaki, *J. Mater. Sci. Lett.*, vol. 16, no. 7, pp. 553–556, Apr. 1997.

[50] T. Yoshitake, G. Shiraishi, and K. Nagayama, *Appl. Surf.Sci.*, vol. 197/198, pp. 379–383, 2002.

[51] J. Patscheider, T. Zehnder, M. Disserens, Surf. Coat. Technol. 146–147 (2001) 201–208.

[52] S. Veprek, Surf. Coat. Technol. 97 (1997) 15.

[53] M. Diserens, J. Patscheider, F. Levy, Surf. Coat. Technol. 120–121 (1999) 158.

[54] K.H. Kim, B.H. Park, Chem. Vapor Depos. 5 (6) (1999) 275.

[55] F. Vaz, L. Rebouta, P. Goudeau, J. Pacaud, H. Garem, J.P. Riviere, A. Cavaleiro, E. Alves, Surf. Coat. Technol. 133–134 (2000) 307.

[56] W.-D. Munz, J. Vac. Sci. Technol. A 4(6) (1986) 2717

[57] O. Knotek, M. Bohmer, T. Leyendecker, J. Vac. Sci. Technol. A 4(6) (1986) 2695.

[58] S. Veprek, J. Vac. Sci. Technol. A 17 (5) (1999) 2401.

[59] S. Zhang, D. Sun, Y. Fu, H. Du, Surf. Coat. Technol. 167 (2003) 113–119.

[60] S.H. Kim, J.K. Kim, K.H. Kim, Thin Solid Films 420–421 (2002) 360.

[61] J.B. Choi, K. Cho, M.-H. Lee, K.H. Kim, Thin Solid Films 447–448 (2004) 365–370.

[62] Y H Cheng, T Browne, B Heckerman, P Gannon, J C Jiang, E I Meletis, C Bowman and V Gorokhovsky, J. Phys. D: Appl. Phys. 42 (2009) 125415

[63] Lughi V and Clarke D R 2006 *Appl. Phys. Lett.* 24 241911

[64] M.C. Polo, J.L. Andujar, A. Hart, J. Robertson, W.I. Milne, Diamond Relat. Mater. 9 (2000) 663-667.

[65] Sung Ryong Choi, In-Wook Park, Sang Ho Kim and Kwang Ho Kim, Thin Solid Films 447 –448 (2004) 371–376

[66] H. Han, F. Ryan, M. McClure, Surf. Coat. Technol. 120 (1999) 579-584.

[67] P.C. Johnson, in: M.H. Francombe, J.L. Vossen (Eds.), Contemporary Preparative Techniques, Academic Press, London, 1989, p.129.

[68] S.Veprek, S.Reiprich, L. Shizhi, Appl.Phys. Lett. 66 (1995) 2640.
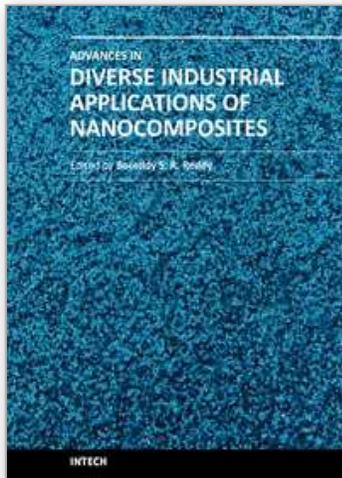
Advances in Diverse Industrial Applications of Nanocomposites
Edited by Dr. Boreddy Reddy

Nanocomposites are attractive to researchers both from practical and theoretical point of view because of combination of special properties. Many efforts have been made in the last two decades using novel nanotechnology and nanoscience knowledge in order to get nanomaterials with determined functionality. This book focuses on polymer nanocomposites and their possible divergent applications. There has been enormous interest in the commercialization of nanocomposites for a variety of applications, and a number of these applications can already be found in industry. This book comprehensively deals with the divergent applications of nanocomposites comprising of 22 chapters.

How to reference

In order to correctly reference this scholarly work, feel free to copy and paste the following:

Seunghun Lee, Do-Geun Kim, Igor Svadkovski and Jong-Kuk Kim (2011). Nanocomposite Films Deposition by means of Various Filtered Vacuum Arc Systems, Advances in Diverse Industrial Applications of Nanocomposites, Dr. Boreddy Reddy (Ed.), ISBN: 978-953-307-202-9, InTech, Available from: http://www.intechopen.com/books/advances-in-diverse-industrial-applications-of-nanocomposites/nanocomposite-films-deposition-by-means-of-various-filtered-vacuum-arc-systems

INTECH
open science | open minds